Cardiovascular Research Advance Access published February 2, 2008

Cardiovascular Research
doi:10.1093/cvr/cvm115

Molecular imaging of $\alpha_v\beta_3$ integrin expression in atherosclerotic plaques with a mimetic of RGD peptide grafted to Gd-DTPA†

Carmen Burtea[1], Sophie Laurent[1], Oltea Murariu[1], Dirk Rattat[2], Gérard Toubeau[3], Alfons Verbruggen[2], David Vansthertem[3], Luce Vander Elst[1], and Robert N. Muller[1]*

[1]*Department of General, Organic and Biomedical Chemistry, NMR and Molecular Imaging Laboratory, University of Mons-Hainaut, 24, Avenue du Champ de Mars, B-7000 Mons, Belgium;* [2]*Laboratory of Radiopharmacy, Department of Pharmaceutical Sciences, Catholic University of Louvain, Onderwijs en Navorsing 2, Box 821, B-3000 Leuven, Belgium; and* [3]*Department of Histology, University of Mons-Hainaut, 24, Avenue du Champ de Mars, B-7000 Mons, Belgium*

Received 31 July 2007; revised 12 December 2007; accepted 21 December 2007

Time for primary review: 23 days

KEYWORDS
Atherosclerosis;
Angiogenesis;
Inflammation;
NMR

Aims The integrin $\alpha_v\beta_3$ is highly expressed in atherosclerotic plaques by medial and intimal smooth muscle cells and by endothelial cells of angiogenic microvessels. In this study, we have assessed non-invasive molecular magnetic resonance imaging (MRI) of plaque-associated $\alpha_v\beta_3$ integrin expression on transgenic ApoE$^{-/-}$ mice with a low molecular weight peptidomimetic of Arg-Gly-Asp (mimRGD) grafted to gadolinium diethylenetriaminepentaacetate (Gd-DTPA-g-mimRGD). The analogous compound Eu-DTPA-g-mimRGD was employed for an *in vivo* competition experiment and to confirm the molecular targeting. The specific interaction of mimRGD conjugated to Gd-DTPA or to ^{99m}Tc-DTPA with $\alpha_v\beta_3$ integrin was furthermore confirmed on Jurkat T lymphocytes.

Methods and results The mimRGD was synthesized and conjugated to DTPA. DTPA-g-mimRGD was complexed with $GdCl_3{\cdot}6H_2O$, $EuCl_3{\cdot}6H_2O$, or with $[^{99m}Tc(CO)_3(H_2O)_3]^+$. MRI evaluation was performed on a 4.7 T Bruker imaging system. Blood pharmacokinetics of Gd-DTPA-g-mimRGD were assessed in Wistar rats and in c57bl/6j mice. The presence of angiogenic blood vessels and the expression of $\alpha_v\beta_3$ integrin were confirmed in aorta specimens by immunohistochemistry. Gd-DTPA-g-mimRGD produced a strong enhancement of the external structures of the aortic wall and of the more profound layers (possibly tunica media and intima). The aortic lumen seemed to be restrained and distorted. Pre-injection of Eu-DTPA-g-mimRGD diminished the Gd-DTPA-g-mimRGD binding to atherosclerotic plaque and confirmed the specific molecular targeting. A slower blood clearance was observed for Gd-DTPA-g-mimRGD, as indicated by a prolonged elimination half-life and a diminished total clearance.

Conclusion The new compound is potentially useful for the diagnosis of vulnerable atherosclerotic plaques and of other pathologies characterized by $\alpha_v\beta_3$ integrin expression, such as cancer and inflammation. The delayed blood clearance, the significant enhancement of the signal-to-noise ratio, and the low immunogenicity of the mimetic molecule highlight its potential for an industrial and clinical implementation.

1. Introduction

Atherosclerosis is an inflammatory disease that may persist for several years before the appearance of clinical manifestations such as heart attack, stroke, or peripheral arterial disease. In addition, many individuals develop coronary heart disease in the absence of abnormal lipoprotein profiles. Despite advances in treatment and preventive programmes, clinical complications of advanced atherosclerosis remain the primary cause of death in Western countries.[1]

At present, clinicians do not dispose of reliable methods to characterize atherosclerotic plaque composition and current clinical decisions remain largely based on location and degree of stenosis.[2] Recent studies have shown that magnetic resonance imaging (MRI) could allow the differentiation of plaque components and the quantification of the degree of luminal narrowing.[3] However, acute coronary syndromes often result from plaque rupture at sites mostly normal or only characterized by modest luminal narrowing

† Parts of this work have been presented at the 23rd Annual Meeting of ESMRMB Warsaw, Poland, 22–28 September 2006.

* Corresponding author. Tel/fax: +32 65 373520.
E-mail address: robert.muller@umh.ac.be

under angiographic examination.[4] Remodelling of the vessel wall often occurs at apparently normal sites, devoid of detectable stenosis.[5] In this context, there is an urgent need for diagnostic procedures dedicated to a specific identification of rupture-prone and vulnerable plaques, which are the most frequent cause of sudden cardiac events.[6] One of the most promising developments in vulnerable plaque diagnosis is the use of contrast agents able to specifically target plaque components, cell surface receptors, or other biomolecules. Indeed, the progression of atherosclerotic plaque disease involves a wide variety of biological mechanisms that could be visualized with targeted MRI or nuclear probes.[7]

One of the most important hallmarks of atherosclerotic vessels is the development of microvascular networks of vasa vasorum extending deeply from the adventitia and outer media towards the intima. This mechanism of plaque angiogenesis seems to be activated by macrophages, T cells, and mast cells. The close proximity of plaque vessels to inflammatory cells and the expression of adhesion molecules on the endothelium of these microvascular networks suggest that they are regulated by a positive feedback mechanism. In addition, the development of such plaque microvessels could represent an essential requirement to sustain plaque growth by supplying oxygen and nutrients, which cannot reach anymore the deepest layers of the artery wall by simple diffusion.[8,9]

The integrin family of adhesion molecules is represented by heterodimeric glycoproteins composed of α and β subunits (currently 15 α and 8 β known subunits). In atherosclerosis, these adhesion molecules have distinct roles in inflammatory cell recruitment to the damaged vessel wall. Multiple ligands can bind to $\alpha_v\beta_3$ integrin in an Arg-Gly-Asp (RGD)-dependent manner. The integrin mediates cell locomotion and is also involved in cell migration through the extracellular matrix.[10–12] The integrin $\alpha_v\beta_3$ seems to be a critical molecule for several processes involved in atherosclerosis progression and in restenosis, e.g. smooth muscle cell (SMC) migration and angiogenesis, as suggested by its prominent expression on microvessels in the adventitia and in the plaque.[13]

The $\alpha_v\beta_3$ integrin has been extensively investigated for imaging of tumour neovascularization.[14] For non-invasive molecular imaging of plaque-associated angiogenesis, Winter *et al.*[15] have developed a paramagnetic nanoparticle contrast agent targeted specifically to $\alpha_v\beta_3$ integrins. These nanoparticles were $\sim$273 nm in diameter, contained $\sim$94 200 Gd^{3+} atoms per particle, and were characterized by a longitudinal relaxivity (r_1) of 17.7 s^{-1} $mmol^{-1}$ L at 1.5 T and room temperature. Although very efficient from the relaxometric point of view, this contrast agent has the drawback of a large size that limits not only its blood clearance, but also its diffusion into the targeted tissue.[16] In fact, $\alpha_v\beta_3$ integrin is expressed both at the sites of angiogenesis and on SMCs accumulated in atherosclerotic plaques.[13]

In the present work, we have assessed non-invasive molecular imaging of plaque-associated angiogenesis with a low molecular weight non-peptidic RGD mimetic[17,18] conjugated to gadolinium diethylenetriaminepentaacetate (Gd-DTPA-g-mimRGD). The RGD mimetic has been reported to inhibit vitronectin and fibrinogen binding to the immobilized $\alpha_v\beta_3$ with an IC_{50} of 3×10^{-10} M.[17] This new compound, targeted to $\alpha_v\beta_3$ integrin, was evaluated by MRI *in vivo* in apolipoprotein E-deficient ($ApoE^{-/-}$) mice. The specific *in vivo* molecular targeting was confirmed by a competition experiment in the presence of the analogous compound Eu-DTPA-g-mimRGD. The specific interaction of mimRGD conjugated to Gd-DTPA or to ^{99m}Tc-DTPA with $\alpha_v\beta_3$ integrin was furthermore confirmed on Jurkat T lymphocytes. Blood pharmacokinetics of Gd-DTPA-g-mimRGD were assessed in Wistar rats and in c57bl/6j mice.

2. Methods

2.1 Reagents

2-(4-Isothiocyanatobenzyl)-diethylenetriaminepentaacetic acid (*p*-SCN-Bn-DTPA) used to obtain Gd-DTPA-g-mimRGD was acquired from Macrocyclics (Dallas, TX, USA). RP-C18 stationary phase used for ligand purification was purchased from Merck (Darmstadt, Germany). IsolinkTM kit used to obtain ^{99m}Tc-DTPA-g-mimRGD was purchased from Tyco Healthcare (Petten, The Netherlands). For Jurkat cell culture, the RPMI 1640 medium was obtained from Sigma-Aldrich (Bornem, Belgium), while the newborn calf serum (NCS) and the antibiotic–antimicotic were purchased from Invitrogen (Merelbeke, Belgium). To stimulate integrin expression, phorbol 12-myristate 13-acetate (PMA, Sigma-Aldrich) was used. GRGD peptide used for competition experiments was from MP Biomedicals (Brussels, Belgium) and from Bachem (Bubendorf, Switzerland). Sodium pentobarbital (Nembutal, Sanofi, Brussels, Belgium) was used to anaesthetize the animals. For immunohistochemistry, the following antibodies and reagents were used: rat anti-mouse integrin α_v (CD51) monoclonal antibody (Chemicon, Heule, Belgium); rat anti-mouse PECAM-1 (platelet endothelial cell adhesion molecule-1, CD31) biotin-conjugated monoclonal antibody (Chemicon); rabbit anti-VCAM-1 (vascular cell adhesion molecule-1) polyclonal antibody (Santa Cruz Biotechnology, Heidelberg, Germany); rat anti-mouse Mac-3 antibody (Sanbio, Uden, The Netherlands); rabbit anti-rat biotinylated IgG, goat anti-biotin IgG, and horse peroxidase-conjugated anti-goat IgG were from Vector Labconsult (Brussels, Belgium); biotinylated goat anti-rabbit IgG (Vector Labconsult); endogenous biotin blocking kit (Invitrogen); and streptavidin-linked peroxidase complexes (ABC kit, DakoCytomation SAS, Trappes, France).

2.2 Synthesis and physico-chemical characterization of DTPA-g-mimRGD complexed with Gd, Eu, or ^{99m}Tc

The RGD mimetic (mimRGD) was obtained as described by Sulyok *et al.*[17] Synthesis was performed on a solid support using the Fmoc strategy.[18] The molecule was coupled with DTPA by reaction between *p*-SCN-Bn-DTPA and the mimetic in aqueous solution (pH 10.0) using a described procedure.[19]

The ligand was purified by column chromatography on a RP-C18 stationary phase with H_2O/methanol (50/50) as the mobile phase. DTPA-g-mimRGD (*Figure 1*) was then complexed with $GdCl_3 \cdot 6H_2O$ or with $EuCl_3 \cdot 6H_2O$. The absence of free lanthanide ions was checked with arsenazo (III) indicator.[20] The mass of the complexes was confirmed by ESI-MS. Gd-DTPA-g-mimRGD: $m/z = 1224$ ($[M + H]^+$) and 1246 ($[M + Na]^+$). Eu-DTPA-g-mimRGD: $m/z = 1218$ ($[M + H]^+$) and 1240 ($[M + Na]^+$). Mass spectra were obtained on a Q-tof 2 mass spectrometer (Micromass, Manchester, UK).

^{99m}Tc-DTPA-g-mimRGD was obtained by mixing 2 mg DTPA-g-mimRGD in 0.2 mL water with 0.2 mL of a $[^{99m}Tc(CO)_3]^+$ solution of pH 10 (400–600 MBq), prepared using an Isolink^{TM} kit, and heating the mixture for 30 min at 40°C, yielding 80% of the technetium-99m tricarbonyl complex.

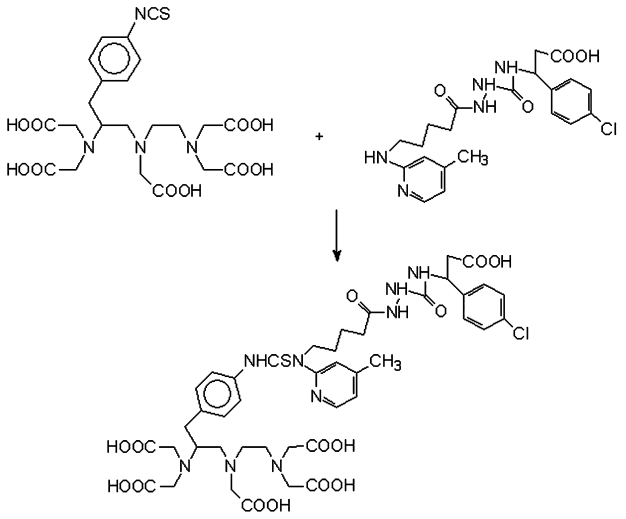

Figure 1 Synthesis of DTPA-mimRGD.

^{99m}Tc(CO)$_3$DTPA, prepared as previously described,[20] was used as a reference and non-specific compound. Both ^{99m}Tc-compounds were analysed using the HPLC method described in ref.[21]

2.3 Validation of the specific interaction with integrins

2.3.1 Culture and stimulation of Jurkat T lymphocytes

Jurkat cells (gift from Prof. Oberdan Leo, Free University of Brussels, IBMM, Gosselies, Belgium) were cultured at a concentration of $1 \times 10^6 mL^{-1}$ in RPMI 1640 medium supplemented with 10% NCS and 1% antibiotic–antimicotic. Cells were resuspended in fresh culture medium prior to exposure to 50 ng PMA/mL for 3 h.

2.3.2 *In vitro* confirmation of integrin binding: Gd-DTPA-g-mimRGD and ^{99m}Tc-DTPA-g-mimRGD

PMA-stimulated and control Jurkat cells ($n = 6$/experimental group) were incubated with MRI (2×10^6 cells/mL; 4 mL/sample) contrast agents (0.4 mM Gd-DTPA-g-mimRGD and Gd-DTPA) or radioactive (10^6 cells/mL; 1.5 mL/sample) tracer agents (0.042 mM ^{99m}Tc-DTPA-g-mimRGD and ^{99m}Tc(CO)$_3$-DTPA) in the culture medium. To confirm the specific binding to integrins, a competition experiment was performed with GRGD peptide at a concentration of 1.55 mM in the case of Gd-DTPA-g-mimRGD and of 2.5 mM in the case of ^{99m}Tc-DTPA-g-mimRGD. After 2 h of incubation at 37°C under mechanical agitation, the cells were rinsed three times with Tris-buffered saline (TBS) buffer (1 mM $CaCl_2$, 2 mM $MgCl_2$, 50 mM Tris–HCl, 150 mM NaCl, and 10 mM Hepes, pH 7.4) (centrifugation for 15 min at 4500 rpm).

For MRI and relaxometric analyses, the final pellet obtained after centrifugation was re-suspended (8×10^6 cells/sample) in 0.1 mL 2% gelatin prepared in phosphate-buffered saline (PBS) (150 mM NaCl, 3.2 mM KCl, 6.4 mM $Na_2HPO_4 \cdot 12\ H_2O$, 1.5 mM KH_2PO_4, pH 7.4) and transferred into 0.2 mL PCR tubes. The samples were then analysed by MRI (Bruker AVANCE-200, 4.7 T, Bruker, Karlsruhe, Germany) using a RARE sequence (TR = 1048.5 ms, TE = 4 ms, RARE factor = 4, NEX = 4, matrix = 256, FOV = 3.5 cm, slice thickness = 1 mm, spatial resolution = 137 μm). The signal intensity (SI) of the images of cell samples was measured using the OSIRIS image analysis software, while their longitudinal relaxation rate values, R_1 ($1/T_1$), were determined at 60 MHz (1.5 T) on a Bruker Minispec mq60. The normalized signal intensity ($SI^{Norm} = SI^{Sample}/SI^{Blank}$) and R_1 ($R_1^{Norm} = R_1^{Sample} - R_1^{Blank}$) were calculated for each cell sample.

The radioactivity of the samples incubated with ^{99m}Tc-DTPA-g-mimRGD or ^{99m}Tc(CO)$_3$-DTPA was measured using a Wallac 1480 WIZARD 3″ automatic gamma counter (Perkin-Elmer, Boston, USA).

2.4 *In vivo* evaluation

All animal experiments were conducted in accordance with the requirements of the Ethics Committee of our institution. The investigation conforms to the Guide for the Care and Use of Laboratory Animals published by the US National Institutes of Health (NIH Publication No. 85-23, revised 1996).

2.4.1 Molecular targeting of atherosclerotic plaques by MRI

2.4.1.1 Animal model of atherosclerosis

Female C57bl/6 ApoE^{tm1unc} mice, aged ~15 months ($n = 10$), were acquired from Charles River Laboratories, Brussels, Belgium. The animals received a Western diet for 3 months before the MRI studies. For MRI experiments, the animals were anaesthetized with 50 mg/kg body weight, ip, of sodium pentobarbital. The contrast agents (Gd-DTPA-g-mimRGD and Gd-DTPA) were injected iv via a caudal vein at a dose of 0.1 mmol/kg. To confirm the specific targeting of $\alpha_v\beta_3$ integrins, an *in vivo* competition experiment ($n = 4$) was performed in the presence of Eu-DTPA-g-mimRGD, which was injected at a dose of 0.1 mmol/kg about 10 min before the administration of Gd-DTPA-g-mimRGD. All images were acquired at the level of the abdominal aorta.

2.4.1.2 MRI equipment and protocols

All experiments were performed on a 200 MHz (4.7 T) AVANCE-200 imaging system equipped with a vertical magnet and a micro-imaging device (Micro2.5AHS/RF, 25 mm coil). A test tube filled with a solution of 0.5 mM Gd-DTPA prepared in 2% gelatin was used as a reference.

The images were acquired with RARE (TR/TE = 1048.5/4 ms, RARE factor = 4, NEX = 4, matrix=256, FOV = 2.3 cm, slice thickness 0.8 mm, 20 axial slices, spatial resolution = 90 μm, TA = 4 min 28 s) and MSME (TR/TE = 695.8/8.9 ms, NEX = 2, FOV = 2.3 × 2.3 cm, matrix = 256 × 256, slice thickness = 1 mm, 20 axial slices, spatial resolution = 90 × 90 μm, TA = 5 min 56 s) imaging protocols. A 3D-TOF sequence (TR/TE = 10/2 ms, flip angle = 20°, NEX = 2, FOV = 4 × 2 × 4 cm, matrix = 256 × 128 × 64, slice thickness = 1 mm, 60 axial slices, spatial resolution = 156 × 156 × 625 μm, TA = 2 min 43 s) was used with the aim to confirm the anatomical localization of the aorta in the image slice.

2.4.1.3 Image analysis

SI values for each time point were measured within regions of interest (ROIs) drawn manually by using the OSIRIS image analysis software in the arterial wall of the abdominal aorta. The ROIs were drawn on serial slices on the area of signal enhancement around the vessel lumen and were reproduced for pre-contrast images, where the aortic wall was not discriminated from the surrounding tissue. The ROIs drawn on a certain mouse were reproduced for each experiment when that animal was submitted to several types of studies, i.e. using Gd-DTPA-g-mimRGD, Gd-DTPA, or Eu-DTPA-g-mimRGD. SI enhancement (ΔSNR%) was calculated according to the following equation:

$$\Delta SNR\% = \frac{(SI_{post}/\text{Noise SD}) - (SI_{pre}/\text{Noise SD})}{(SI_{pre}/\text{Noise SD})} \times 100$$

where SI_{post}, post-contrast SI; SI_{pre}, pre-contrast SI.

The data were averaged and the standard error of the mean (SEM) was calculated for each time point.

2.5 Immunohistochemistry

Aorta specimens were collected subsequent to MRI evaluation. After fixation in 4% buffered paraformaldehyde solution, routine processing, and paraffin embedding, 5 μm thick sections were cut. After

rehydration, endogenous peroxidases were blocked with 0.15% H_2O_2, while endogenous biotin was blocked with a blocking kit.

The expression of $\alpha_v\beta_3$ integrin and the presence of angiogenic blood vessels in aorta specimens were confirmed with rat anti-mouse integrin α_v monoclonal antibody (10 μg/mL), rat anti-mouse PECAM-1 biotin-conjugated monoclonal antibody (5 μg/mL), and rabbit anti-VCAM-1 polyclonal antibody (2 μg/mL); the macrophages were detected with a rat anti-mouse Mac-3 (40 μg/mL).

The sections were incubated overnight with the primary antibodies and for 1 h with secondary IgG. Anti-CD51 and anti-Mac-3 were detected with biotinylated rabbit anti-rat IgG (10 μg/mL). This last one and biotinylated anti-CD31 antibody were followed by goat anti-biotin IgG (5 μg/mL) and horse peroxidase-conjugated anti-goat IgG (1 μg/mL). Anti-VCAM-1 antibody was detected with a biotinylated goat anti-rabbit IgG (10 μg/mL) followed by streptavidin-linked peroxidase complexes.

Finally, the sections were incubated 5 min with 50 mM Tris–HCl, pH 7.4, and then stained with 0.05% 3,3′-diaminobenzidine (DAB) completed with 0.02% H_2O_2 in PBS. The sections were finally counterstained with hemalun and Luxol fast blue and mounted in a permanent medium.

PECAM-1 expression was also evaluated by a protocol adapted from Moulton *et al.*,[8] where CD31 is stained on whole-mount aorta with biotinylated anti-PECAM-1 antibody (5 μg/mL, overnight), followed by streptavidin-linked peroxidase complexes. All incubations were carried out at 4°C. For colour development, aortas were incubated with 0.05% DAB in 50 mM Tris, pH 7.4, for 5 min before adding 0.01% H_2O_2.

The controls were represented by aortas from healthy mice C57bl/6j and samples processed by the same protocols as above, except the primary antibodies.

2.6 Plasma pharmacokinetics

Plasma pharmacokinetics were assessed on Wistar rats ($n = 8$/group, weight 200 g ± 50 g) and on c57bl/6j mice ($n = 3$/blood sampling, weight 24 ± 3 g) (Harlan, Horst, The Netherlands) injected with contrast agents (Gd-DTPA-g-mimRGD and Gd-DTPA) at a dose of 0.1 mmol/kg body weight. Gadolinium content of the blood samples (collected through the carotid artery) was determined by relaxometry at 37°C and 60 MHz on a Bruker Minispec. In the case of Wistar rats, a two-compartment distribution model was used to calculate the pharmacokinetic parameters: the elimination half-life ($T_{e1/2}$), the steady-state volume of distribution (VD_{ss}), and the total clearance (Cl_{tot}). For c57bl/6 mice, the blood plasma concentration was measured at three time points (3, 30, and 60 min, respectively) after the injection of contrast agents and the results were expressed as μmol/L. For each time point, the blood was sampled from a different mouse.

2.7 Statistical analysis

The mean ± SEM were calculated for each experimental group and the statistical significance was evaluated with Student's *t*-test. The results were considered as significant for a $P < 0.05$.

3. Results

3.1 Physicochemical characterization of Gd-DTPA-g-mimRGD

The Gd-complex was characterized *in vitro* by relaxometry in aqueous solution. Proton longitudinal (r_1) relaxivity was measured at 37°C on Bruker Minispecs PC-20 and mq60 (Bruker) and was found to be 4.75 s^{-1} mM^{-1} at 0.47 T and 4.33 s^{-1} mM^{-1} at 1.5 T. The stability of Gd-DTPA-g-mimRGD in blood plasma over time was confirmed by measuring r_1 (0.47 T, 37°C) at various time points during 72 h (Δr_1 in blood plasma/r_1 in water = 1.5 ± 0.04). The absence of any significant interaction with blood plasma proteins was confirmed by measuring the r_1 of Gd-DTPA-g-mimRGD (0.47 T, 37°C) in 4% human serum albumin, HSA ($r_1^{\text{Gd-DTPA-mimRGD-HSA}}/r_1^{\text{Gd-DTPA-mimRGD-H}_2\text{O}} = 1.4 \pm 0.02$).

Transmetallation by zinc(II) ions was evaluated by the decrease of the water longitudinal relaxation rate at 310 K and 20 MHz (Bruker Minispec PC 20) of buffered phosphate solutions (pH 7) containing 2.5 mM of the gadolinium complex and 2.5 mM of $ZnCl_2$.[22] The results shown in *Figure 2* indicate a higher stability of the complex Gd-DTPA-g-mimRGD in comparison with the parent compound, Gd-DTPA. Transmetallation of the gadolinium complex by diamagnetic Zn^{2+} ions in a phosphate-buffered solution is reflected by a decrease of the proton relaxation rate $[R_1^P(t)/R_1^P(0)]$ as a function of time.

3.2 *In vitro* validation of the specific interaction of mimRGD conjugated to DTPA (Gd-DTPA-g-mimRGD and ^{99m}Tc-DTPA-g-mimRGD) with integrins

Gd-DTPA-g-mimRGD was evaluated on Jurkat T cells to confirm the preservation of its affinity for integrins (*Figure 3A*). The MR image shows a higher signal enhancement produced by Gd-DTPA-g-mimRGD on PMA stimulated Jurkat cells ($SI^{Norm} = 2.32$) as compared with non-stimulated cells ($SI^{Norm} = 1.50$) and to the cells incubated with the non-specific contrast agent Gd-DTPA (SI^{Norm} of PMA-stimulated Jurkat cells = 1.33; SI^{Norm} of Jurkat cells non-stimulated with PMA = 1.13); the competition with GRGD peptide has diminished SI^{Norm} ($SI^{Norm} = 1.49$) by 36%, confirming the specific binding of Gd-DTPA-g-mimRGD to Jurkat cells (*Figure 3B*). The R_1^{Norm} measured at 1.5 T attests to the superior binding levels ($P < 0.05$) of Gd-DTPA-g-mimRGD to PMA stimulated cells (0.065 s^{-1}) as compared with various controls, such as non-stimulated cells (0.023 s^{-1}) Gd-DTPA (0.012 s^{-1} for PMA samples and 0.0075 s^{-1} for non-stimulated cells), or cells submitted to competition

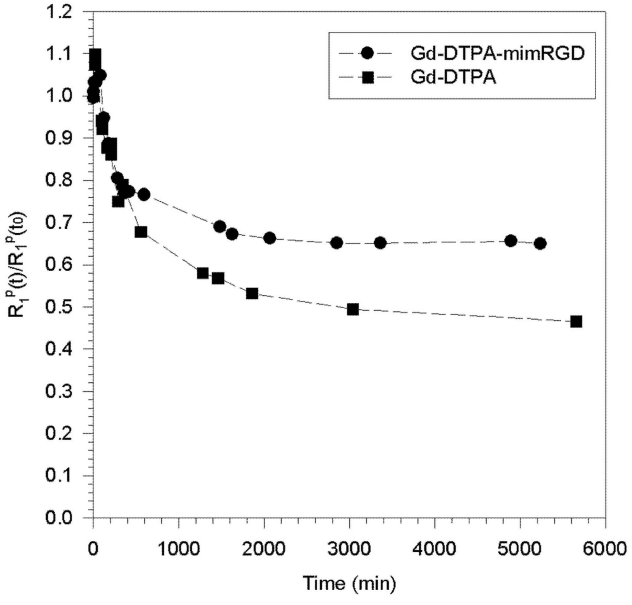

Figure 2 Evolution of the relative water proton paramagnetic longitudinal relaxation rate $R_1^P(t)/R_1^P(0)$ vs. time for Gd-DTPA-g-mimRGD and Gd-DTPA. The higher stability of the complex Gd-DTPA-g-mimRGD compared with that of the parent compound, Gd-DTPA, is indicated by the slower decrease of the proton relaxation rate.

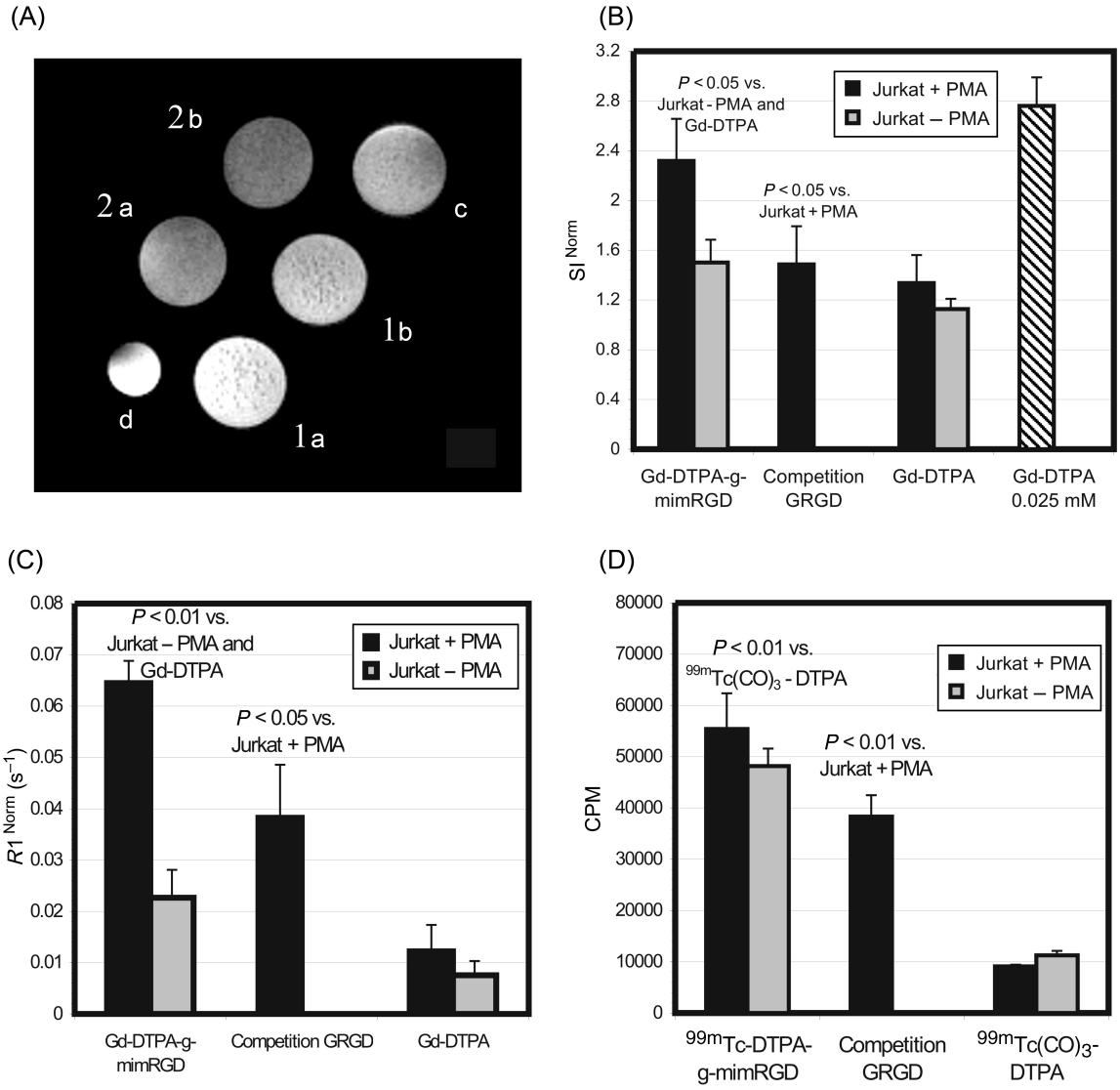

Figure 3 *In vitro* validation of the specific interaction with integrins expressed by Jurkat T lymphocytes of mimRGD conjugated to Gd-DTPA and to ^{99m}Tc-DTPA. MR images of Jurkat cells stimulated with PMA (1a and 2a) or not (1b and 2b) and incubated with 0.4 mM of Gd-DTPA-g-mimRGD (1a and 1b) or with Gd-DTPA (2a and 2b). The test samples are compared with reference samples, i.e. cells in gelatin (c) and 0.025 mM Gd-DTPA in gelatin (d) (*A*). The SI^{Norm} values measured on MR images are represented in (*B*), while the R_1^{Norm} values of the same cell samples measured at 60 MHz are shown in (*C*). The specific binding of DTPA-g-mimRGD to Jurkat cells was furthermore confirmed after labelling with ^{99m}Tc (^{99m}Tc-DTPA-g-mimRGD) (*D*).

(0.038 s^{-1}) (*Figure 3C*). The specific binding of DTPA-g-mimRGD to Jurkat cells was furthermore confirmed ($P <$ 0.01 vs. competing conditions and $^{99m}Tc(CO)_3$-DTPA) after labelling with ^{99m}Tc. ^{99m}Tc-DTPA-g-mimRGD showed 31% lower binding levels in the presence of GRGD peptide (*Figure 3D*).

3.3 Molecular imaging of atherosclerotic plaques with Gd-DTPA-g-mimRGD

Figure 4A shows axial slices at the level of abdominal aorta of an $ApoE^{-/-}$ mouse before and various times after the administration of Gd-DTPA-g-mimRGD. The external structures of aortic wall (tunica media and adventitia) were strongly enhanced 10 min post-contrast; although weaker, this enhancement was still present at 55 min. In the enlarged image of this anatomic slice (*Figure 4B*), the contour of the atherosclerotic wall is visible along with the more profound layers (towards the aortic lumen) of the aortic wall (tunica media and intima). The aortic lumen seems to be restrained and distorted. It is remarkable that the spatial resolution of these images is in the micrometre range, i.e. 90 μm. The same mouse was injected with Gd-DTPA and the post-contrast image is shown in *Figure 4 C*. The anatomic slices are almost in the same position, by taking into account the spinal cord as a reference (the other organs change relatively their position). As compared with Gd-DTPA-g-mimRGD, the enhancement produced by the non-specific contrast agent Gd-DTPA is rather diffuse and the aortic wall is not clearly outlined.

The aorta localization was possible thanks to the MRI protocol 3D-TOF (*Figure 5*), which has also evidenced the backward enhancement of the aortic wall (a clear spot towards the spinal cord). A comparison with the pre-contrast image clearly indicates that this particular enhancement was produced by the contrast agent.

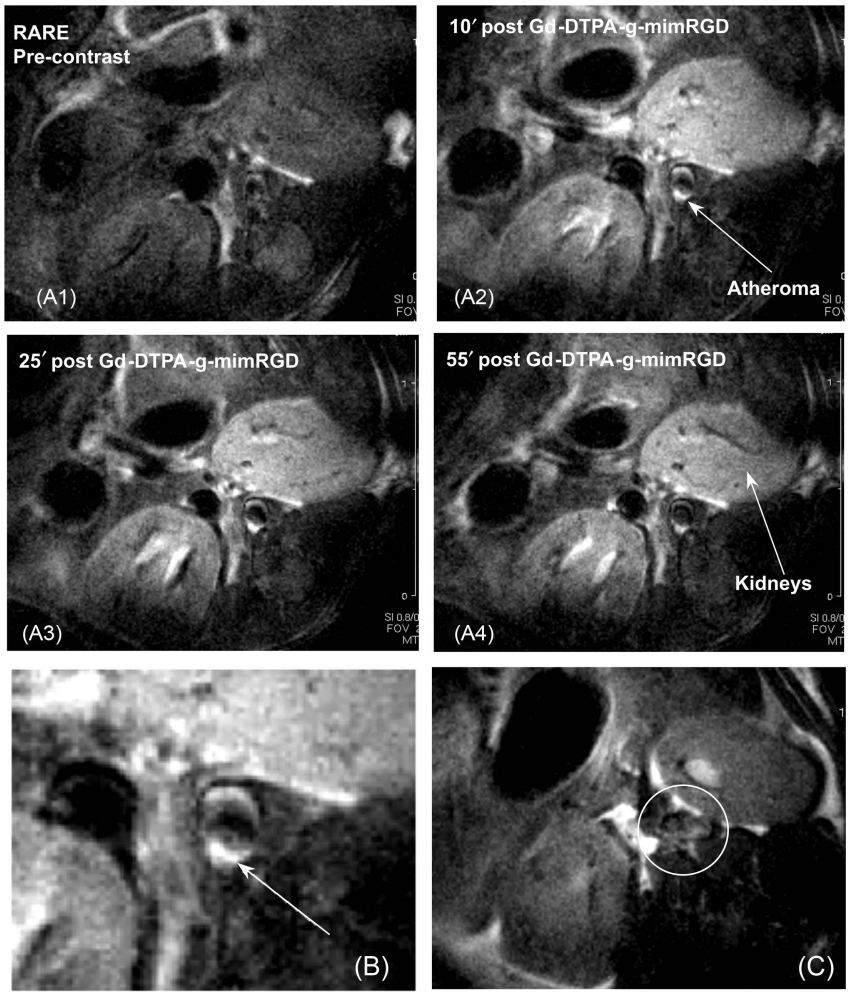

Figure 4 Molecular imaging of atherosclerotic plaque with Gd-DTPA-g-mimRGD: pre-contrast and at 10′, 25′, and 55′ post-contrast (*A*). The image acquired at 10′ post-contrast is enlarged in (*B*) for better resolution of atherosclerotic plaque (indicated by the arrow). For comparison, the image obtained with Gd-DTPA is presented in (*C*).

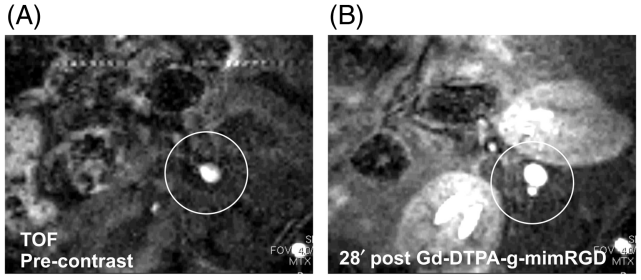

Figure 5 MRI of abdominal aorta before (*A*) and after injection of Gd-DTPA-g-mimRGD (*B*) by using the 3D-TOF imaging protocol.

An *in vivo* competition experiment was designed to validate the specific integrin targeting at the level of atherosclerotic plaques by blocking the receptor with an analogous compound, Eu-DTPA-g-mimRGD, which should not have a significant effect on signal enhancement since its r_1 is very small. The contrast enhancement obtained in non-competing conditions (*Figure 6A*) is compared with that produced in this competition experiment (*Figure 6B*) and to the results obtained with the non-specific contrast agent Gd-DTPA (*Figure 6C*). The histological examination of abdominal aorta harvested after MRI session confirmed the presence of atherosclerotic lesion (disrupted media and thickened intima) and the expression of α_v integrins (*Figure 6D*). Some structures in the disrupted media seem to have a lumen, which probably could be associated with angiogenic neo-vessels; most of them seem to be located at the intima-media border.[8] The signal enhancement of the aortic wall produced in competing or non-specific conditions is 40–90% lower than with Gd-DTPA-g-mimRGD. This effect was either global or restricted to a certain area of the aortic wall. This means that a certain fraction of the contrast agent (specific or non-specific) is free to circulate into the microvascular network of the aortic wall, which explains the relative signal enhancement produced by the non-specific compound, Gd-DTPA. Although low, such a non-specific enhancement could represent a potential drawback for the specific diagnosis of atherosclerotic disease in this particular case. In clinical practice, this could be solved by subtracting the images obtained with a non-specific compound from the ones produced by the specifically targeted contrast agent. This procedure should allow the precise localization of pathological areas expressing the targeted

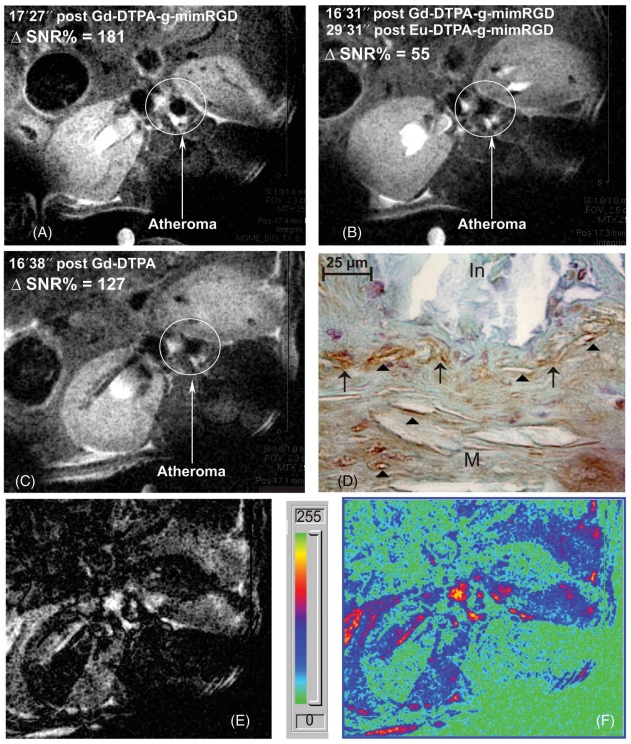

Figure 6 *In vivo* contrast enhancement produced by Gd-DTPA-g-mimRGD in non-competing conditions (*A*) compared with image obtained in the competition experiment (*B*) and to the one obtained with Gd-DTPA (*C*). The presence of atherosclerotic lesion (disrupted media, M, and thickened intima, In) and the expression of α_v integrins (arrows) were confirmed by immunohistochemistry; some structures in the disrupted media seem to have a lumen, which probably could be associated with angiogenic neo-vessels (arrowheads) (*D*). The subtraction of image (*A*) is also shown (*E*) together with colour-coded signal enhancement (*F*).

receptor. An example of this type of image processing is shown in *Figure 6 E* along with colour-coded signal enhancement (*Figure 6F*), which highlights the areas of higher tissue enhancement.

The ΔSNR% is represented as a function of time in *Figure 7*. Gd-DTPA-g-mimRGD produced at 42 min post-contrast a maximum signal enhancement (147%), which thereafter decreased progressively, although remaining at 97% 105 min post-contrast. In the presence of Eu-DTPA-g-mimRGD, ΔSNR% did not surpass the level produced by the non-specific Gd-DTPA and ranged between 75 and 15%.

3.4 Immunohistochemistry

Immunohistochemistry studies on aorta specimens harvested after MRI sessions confirmed the expression of VCAM-1 (*Figure 8A*), PECAM-1 (*Figure 8B*), and Mac-3 (*Figure 8C*). VCAM-1 and PECAM-1 are often expressed around capillary-like structures, most of them located at the intima-media border. Mac-3 confirms the invasion of the aortic wall by macrophages, which were detected both in intima and in media layers.

Figure 8D shows a control aorta harvested from a C57bl/6j mouse, immunostained for PECAM-1 expression. The internal elastic membrane is visible, with a scalloped appearance, and the endothelial cells (endothelial nuclei) appear to rest directly on it. No PECAM-1 expression could be detected on the endothelial layer probably because the

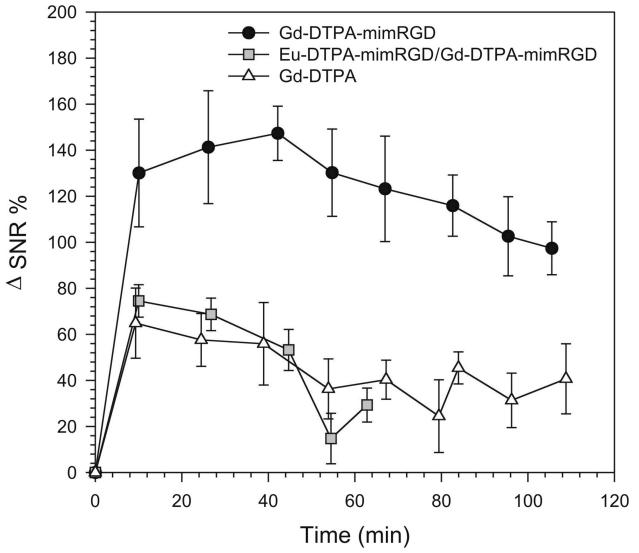

Figure 7 Time evolution of ΔSNR% of atherosclerotic plaque in ApoE$^{-/-}$ mice treated with Gd-DTPA-g-mimRGD in the absence and in the presence of Eu-DTPA-g-mimRGD as a competitor and comparison with Gd-DTPA.

integrity of endothelial cells was lost during histological processing.

The presence of vasa vasorum networks immunostained for PECAM-1 expression, which are probably angiogenic, was identified on whole-mount aorta from ApoE$^{-/-}$ mice (*Figure 8E*), but not on that from control c57bl/6j mice (*Figure 8F*).

3.5 Pharmacokinetic characterization

A slower blood clearance was observed for Gd-DTPA-g-mimRGD, as proven by the prolonged $T_{e1/2}$ and the diminished total clearance (*Table 1*). The VD_{ss} of Gd-DTPA-g-mimRGD is not significantly different from that of Gd-DTPA. In mice, the kinetics of blood plasma concentration (*Table 2*) suggest a delayed clearance at 30 min (350 μmol/L for Gd-DTPA-g-mimRGD vs. 268 μmol/L for Gd-DTPA) and at 60 min (224 μmol/L for Gd-DTPA-g-mimRGD vs. 168 μmol/L for Gd-DTPA), respectively, after the injection of the contrast agents.

4. Discussion

The costs related to coronary heart disease and stroke in the USA were estimated to exceed 180 billion US$ in 2004.[23] In Europe, cardiovascular disease accounts for almost half of deaths and is estimated to cost the EU economy €169 billion/year.[24] Epidemiological studies have revealed that many patients with sudden cardiac events do not show preliminary cardiovascular symptoms. Accordingly, the diagnosis of vulnerable atherosclerotic plaques represents one of the main objectives in the prevention and treatment of cardiovascular disease.

Among the contemporary methods of medical imaging, MRI offers the unique advantage of being non-invasive and furnishing simultaneously, and with a high spatial resolution, anatomical, physiological, and molecular information. Nevertheless, the quite low efficiency of MRI contrast agents represents a challenge with respect to the choice of the most adequate method of chemical synthesis and to

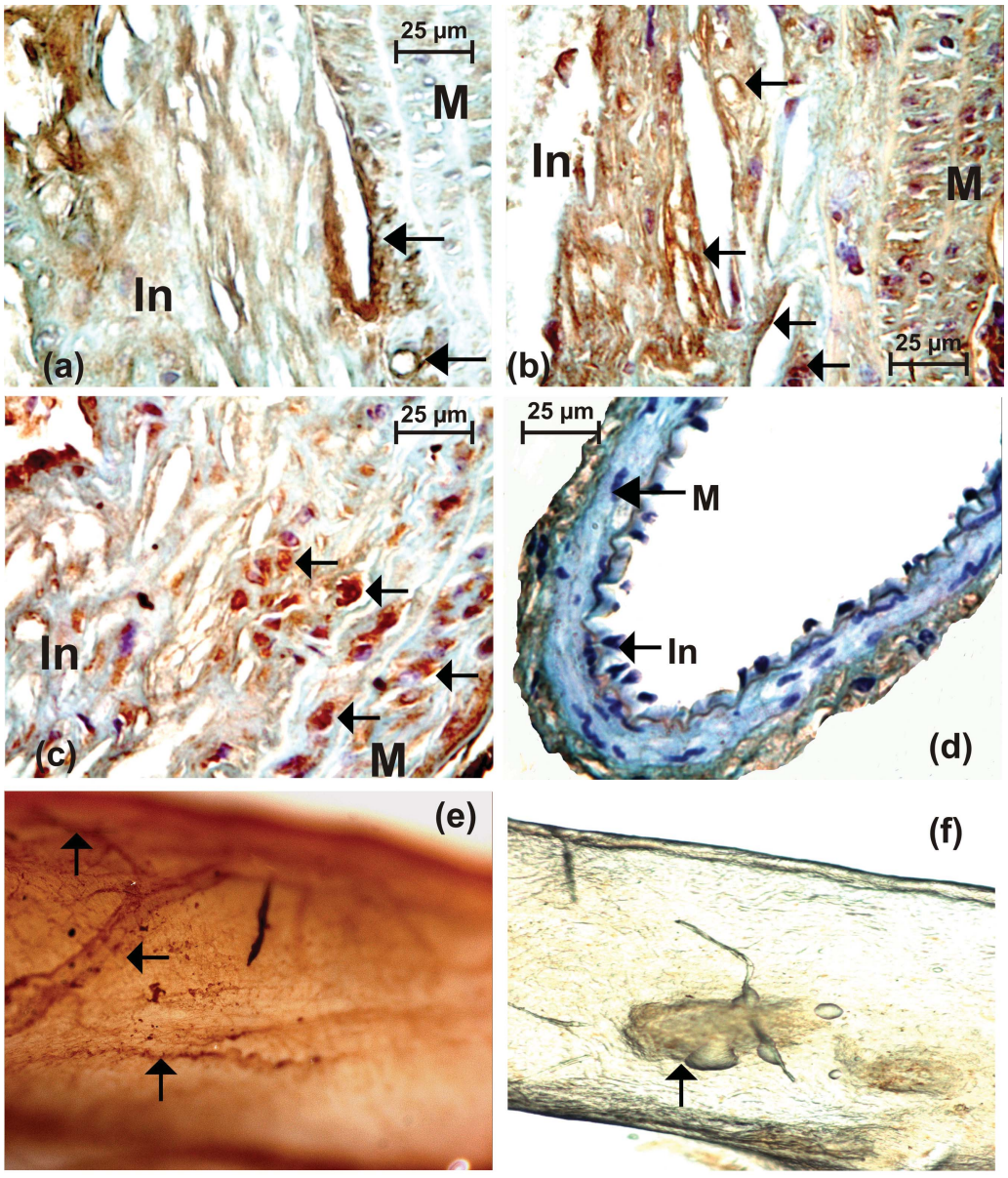

Figure 8 Immunohistochemistry of VCAM-1 (*A*), PECAM-1 (*B*), and Mac-3 (*C*) expression stained in brown and dark-brown (pointed by arrows) in tunica media (M) and intima (In) on paraffin-embedded sections of aorta from ApoE$^{-/-}$ mice; no PECAM-1 expression could be detected on aorta from control C57bl/6j mice (*D*). The vasa vasorum networks (pointed by arrows), probably angiogenic, were immunostained for PECAM-1 expression on whole-mount aorta from ApoE$^{-/-}$ mice (*E*), but no evident vasa vasorum network could be observed on control aorta from C57bl/6j mice (*F*); the arrow points to a branch of the aorta.

Table 1 Pharmacokinetic parameters of Gd-DTPA-g-mimRGD as compared with Gd-DTPA determined in Wistar rats

Contrast agent	$T_{e1/2}$ (min)	Cl_{tot} (mL/kg/min)	VD_{ss} (L/kg)
Gd-DTPA-g-mimRGD	57.2 ± 9.1**	4.8 ± 1.1**	0.304 ± 0.024
Gd-DTPA	20.8 ± 6.1	7.9 ± 1.5	0.247 ± 0.07

**$P < 0.01$ vs. Gd-DTPA.

Table 2 Kinetics of blood plasma concentration of Gd-DTPA-g-mimRGD as compared with Gd-DTPA determined in C57bl/6j mice

Time (min)	Blood plasma concentration (μmol/L)	
	Gd-DTPA-g-mimRGD	Gd-DTPA
3	694 ± 90	658 ± 11
30	350 ± 23	268 ± 10
60	224 ± 5	168 ± 3

the development of MRI protocols adapted to their detection.

The MRI techniques using commercially available extracellular contrast agents have often improved plaque characterization. They helped discriminating the fibrous cap from the lipid core, while the degree of plaque enhancement was found to correlate with that of the neovascular network.[25,26]

The new generation of MR contrast agents dedicated to molecular imaging seems to be quite promising for the diagnosis of vulnerable plaques due to their vectorization with a molecular moiety able to target a pathologically overexpressed biomolecule. Due to the low tissue concentrations of these biomolecules, the current opinion is that the success of MR molecular imaging highly depends on the relaxivity of magnetic reporters. Higher proton relaxivity is often achieved by increasing the molecular mass of the paramagnetic contrast agent, which slows down its rotational motion.[27] The low molecular weight compounds represent a potential alternative, because their proton relaxivity will increase after target binding, enhancing thus the efficiency of MRI detection. A classical example is that of the blood-pool contrast agent MS-325, which shows a nine-fold increase of relaxivity in the albumin-bound form.[28]

The low molecular weight MRI contrast agent developed in the present work was vectorized to $\alpha_v\beta_3$ integrin expressed in atherosclerotic plaques due to a RGD peptidomimetic that was conjugated to Gd-DTPA. Presenting a high specific affinity for $\alpha_v\beta_3$ integrin, the RGD mimetic is binding to PMA-stimulated Jurkat T lymphocytes with an apparent dissociation constant, K^*_d, of 1.13×10^{-8} M after conjugation to USPIO.[18]

By considering the relatively small relaxivity of our integrin-targeted paramagnetic contrast agent and the receptor concentration ($\sim 1.3 \times 10^{-8}$ M, if we consider $\sim 10^5$ receptors/cell and 8×10^6 cells/0.1 mL), the SI enhancement of cell samples is explained by the binding of Gd-DTPA-g-mimRGD to cell receptors, with a subsequent increase of relaxation rate resulting from the slowing down of its rotational motion. This is confirmed by the R_1^{Norm} measured at 1.5 T, since its value surpasses the one expected for a nanomolar concentration of the targeted receptors.

The competition experiment with the GRGD peptide confirmed the specific integrin binding of mimRGD to Jurkat T lymphocytes both when conjugated to USPIO (65–77% inhibition of binding),[18] Gd-DTPA (36% inhibition of binding) or to $^{99m}Tc(CO)_3$-DTPA (31% inhibition of binding).

In atherosclerotic plaques, the integrin $\alpha_v\beta_3$ is highly expressed by medial and intimal SMCs and by endothelial cells of angiogenic microvessels.[13] Our $\alpha_v\beta_3$-targeted contrast agent, Gd-DTPA-g-mimRGD, strongly enhanced the external layers of the aortic wall, probably corresponding to the microvascular network of vasa vasorum. The more profound layers were also delineated, possibly as a result of a specific interaction with the targeted receptor expressed not only by angiogenic microvessels, but also by the intimal SMCs. The specific imaging of integrin expression is sustained by the lower and diffuse signal enhancement of the aortic wall produced in competing conditions or with a non-specific compound (Gd-DTPA). As shown above, part of the signal enhancement is produced by the free diffusion of the contrast agent through the microvascular network of the artery's wall. Such a potential drawback for the molecular imaging of any particular receptor could be solved in clinical practice by subtracting the images obtained with a non-specific compound from those produced by specifically targeted contrast agents. Another possible limitation is represented by the expression of $\alpha_v\beta_3$ integrin by both normal arteries and atherosclerotic plaques.[7,13] Nevertheless, the implementation of contrast agents targeted to specific plaque constituents together with MRI morphometric techniques developed lately along with dedicated surface coils and high-field clinical systems could concomitantly allow the measurement of intima-media thickness and evaluate specifically the plaque's vulnerability.[2,29,30]

The presence of atherosclerotic plaques was confirmed on histological specimens, which have shown the expression of α_v integrins, VCAM-1 and PECAM-1, and probably the presence of angiogenic vasa vasorum networks. The immunostaining of these adhesion molecules was positive predominantly at the intima-media border around capillary-like structures, but also in the modified intima, although with a more sparse distribution. However, it has already been well documented that the expression of these adhesion molecules is not only an attribute of endothelial cells, but also of various leukocytes involved in the atherosclerotic lesion such as monocytes/macrophages, platelets and a subpopulation of T lymphocytes. The immunostaining of Mac-3 in our aorta specimens has confirmed the invasion of the aortic wall by macrophages. Our results corroborate the data in literature, where the role of angiogenesis in plaque progression and complication has been extensively investigated and confirmed both in humans and in $ApoE^{-/-}$ mice.[8–10]

The $\alpha_v\beta_3$-targeted contrast agent is characterized by a slower blood clearance as compared with that of Gd-DTPA, which represents an advantage for molecular imaging of atherosclerotic blood vessels by extending the time-window of MRI scans. The significant enhancement of the signal/noise ratio and the low immunogenicity of the mimetic molecule highlight its potential for an industrial and clinical implementation. Thus, the new contrast agent could contribute to high-resolution *in vivo* molecular imaging methods, aimed at the localization and quantification of unstable atherosclerotic lesions.

Acknowledgements

The authors thank Mrs Patricia de Francisco for her help in preparing the manuscript.

Conflict of interest: none declared.

Funding

This work was financially supported by the FNRS and the ARC (research contract nos 00/05-258 and 05/10-335) Programmes of the French Community of Belgium. The FNRS programme is gratefully acknowledged for the upgrade of the AVANCE-200 imaging system. The EMIL Network of Excellence of the 6th Framework Programme of the European Community is kindly acknowledged.

References

1. Libby P. Inflammation in atherosclerosis. *Nature* 2002;**420**:868–874.
2. Leiner T, Gerretsen S, Botnar R, Lutgens E, Cappendijk V, Kooi E *et al*. Magnetic resonance imaging of atherosclerosis. *Eur Radiol* 2005;**15**: 1087–1099.
3. Briley-Saebo KC, Mulder WJ, Mani V, Hyafil F, Amirbekian V, Aguinaldo JG *et al*. Magnetic resonance imaging of vulnerable atherosclerotic plaques: current imaging strategies and molecular imaging probes. *J Magn Reson Imaging* 2007;**26**:460–479.

4. Myerburg RJ, Interian A Jr, Mitrani RM, Kessler KM, Castellanos A. Frequency of sudden cardiac death and profiles of risk. *Am J Cardiol* 1997; **80**:10F–19F.
5. Fuster V, Badimon L, Badimon JJ, Chesebro JH. The pathogenesis of coronary artery disease and the acute coronary syndromes (1). *N Engl J Med* 1992;**326**:242–250.
6. Glagov S, Weisenberg E, Zarins CK, Stankunavicius R, Kolettis GJ. Compensatory enlargement of human atherosclerotic coronary arteries. *N Engl J Med* 1987;**316**:1371–1375.
7. Jaffer FA, Libby P, Weissleder R. Molecular and cellular imaging of atherosclerosis—emerging applications. *J Am Coll Cardiol* 2006;**47**:1328–1338.
8. Moulton KS, Vakili K, Zurakowski D, Soliman M, Butterfield C, Sylvin E *et al*. Inhibition of plaque neovascularization reduces macrophage accumulation and progression of advanced atherosclerosis. *Proc Natl Acad Sci USA* 2003;**100**:4736–4741.
9. de Boer OJ, Wal van der AC, Teeling P, Becker AE. Leucocyte recruitment in rupture prone regions of lipid-rich plaques: a prominent role for neovascularization? *Cardiovasc Res* 1999;**41**:443–449.
10. Clyman RI, Mauray F, Kramer RH. Integrins have different roles in the adhesion and migration of vascular smooth muscle cells on extracellular matrix. *Exp Cell Res* 1992;**200**:272–284.
11. Weerasinghe D, McHugh KP, Ross FP, Brown EJ, Gisler RH, Imhof BA. A role for the $\alpha_v\beta_3$ integrin in the transmigration of monocytes. *J Cell Biol* 1998; **142**:595–607.
12. Hillis GS, Flapan AD. Cell adhesion molecules in cardiovascular disease: a clinical perspective. *Heart* 1998;**79**:429–431.
13. Hoshiga M, Alpers CE, Smith LL, Giachelli CM, Schwartz SM. Alpha-v beta-3 integrin expression in normal and atherosclerotic artery. *Circ Res* 1995;**77**:1129–1135.
14. Anderson SA, Rader RK, Westlin WF, Null C, Jackson D, Lanza GM *et al*. Magnetic resonance contrast enhancement of neovasculature with $\alpha_v\beta_3$-targeted nanoparticles. *Magn Reson Med* 2000;**44**:433–439.
15. Winter PM, Morawski AM, Caruthers SD, Fuhrhop RW, Zhang H, Williams TA *et al*. Molecular imaging of angiogenesis in early-stage atherosclerosis with $\alpha_v\beta_3$-integrin-targeted nanoparticles. *Circulation* 2003; **108**:2270–2274.
16. Okuhata Y. Delivery of diagnostic agents for magnetic resonance imaging. *Adv Drug Deliv Rev* 1999;**37**:121–137.
17. Sulyok GA, Gibson C, Goodman SL, Holzemann G, Wiesner M, Kessler H. Solid-phase synthesis of a nonpeptide RGD mimetic library: new selective alpha-v-beta-3 integrin antagonists. *J Med Chem* 2001;**44**:1938–1950.
18. Burtea C, Laurent S, Roch A, Vander Elst L, Muller RN. C-MALISA (Cellular Magnetic-Linked Immunosorbent Assay), a new application of cellular ELISA for MRI. *J Inorg Biochem* 2005;**99**:1135–1144.
19. Henoumont C, Henrotte V, Laurent L, Vander Elst L, Muller RN. Synthesis of a new gadolinium complex with a high affinity for human serum albumin and its manifold physicochemical characterization by proton relaxation rate analysis, NMR diffusometry and electrospray mass spectrometry. *J Inorg Biochem* 2007, doi: 10.1016/j.jinorgbio.2007.10.017.
20. Barge A, Cravotto G, Gianolio E, Fedeli F. How to determine free Gd and free ligand in solution of Gd chelates. A technical note. *Contrast Med Mol Imaging* 2006;**1**:184–188.
21. Rattat D, Terwinghe C, Verbruggen A. Comparison of 'classic' ^{99m}Tc–DTPA, ^{99m}Tc(CO)3–DTPA and ^{99m}Tc(CO)2(NO)–DTPA. *Tetrahedron* 2005; **61**:9563–9568.
22. Laurent S, Vander Elst L, Copoix F, Muller RN. Stability of MRI paramagnetic contrast media. A proton relaxometric protocol for transmetallation assessment. *Invest Radiol* 2001;**36**:115–122.
23. Leiner T, Gerretsen S, Botnar R, Lutgens E, Cappendijk V, Kooi E *et al*. Magnetic resonance imaging of atherosclerosis. *Eur Radiol* 2005;**15**: 1087–1099.
24. Petersen S, Pero V, Rayner M, Lear J, Luergo-Fernandez R, Gray A. European Cardiovascular Disease Statistics, 2005 edition. *European Heart Network*.
25. Yuan C, Kerwin WS, Ferguson MS, Polissar N, Zhang S, Cai J *et al*. Contrast-enhanced high resolution MRI for atherosclerotic carotid artery tissue characterization. *J Magn Reson Imaging* 2002;**15**: 62–67.
26. Wasserman BA, Smith WI, Trout HH, Cannon RO, Balaban RS, Arai AE. Carotid artery atherosclerosis: in vivo morphologic characterization with gadolinium-enhanced double-oblique MR imaging initial results. *Radiology* 2002;**223**:566–573.
27. Wickline SA, Lanza GM. Nanotechnology for molecular imaging and targeted therapy. *Circulation* 2003;**107**:1092–1095.
28. Muller RN, Raduchel B, Laurent S, Platzek J, Piérart C, Mareski P *et al*. Physicochemical characterization of MS-325, a new gadolinium complex, by multinuclear relaxometry. *Eur J Inorg Chem* 1999; 1949–1955.
29. Adame IM, van der Geest RJ, Bluemke DA, Lima JAC, Reiber JHC, Lelieveldt BPF. Automatic vessel wall contour detection and quantification of wall thickness in in-vivo MR images of the human aorta. *J Magn Reson Imaging* 2006;**24**:595–602.
30. Itskovich VV, Samber DD, Mani V, Aguinaldo JGS, Fallon JT, Tang CY *et al*. Quantification of human atherosclerotic plaques using spatially enhanced cluster analysis of multicontrast-weighted magnetic resonance images. *Magn Reson Med* 2004;**52**:515–523.